Rashba spin splitting and perpendicular magnetic anisotropy of Gd-adsorbed zigzag graphene nanoribbon modulated by edge states under external electric fields

Zhenzhen Qin [1,5,*] Guangzhao Qin [2,3,†] Bin Shao [4,‡] and Xu Zuo [5,§]

[1]*International Laboratory for Quantum Functional Materials of Henan, and School of Physics and Microelectronics, Zhengzhou University, Zhengzhou 450001, China*

[2]*State Key Laboratory of Advanced Design and Manufacturing for Vehicle Body, College of Mechanical and Vehicle Engineering, Hunan University, Changsha 410082, China*

[3]*Department of Mechanical Engineering, University of South Carolina, Columbia, South Carolina 29201, USA*

[4]*Bremen Center for Computational Material Science, Bremen University, Am Fallturm 1, Bremen 28359, Germany*

[5]*College of Electronic Information and Optical Engineering, Nankai University, Tianjin 300350, China*

(Received 23 April 2019; revised manuscript received 1 January 2020; published 31 January 2020)

The one-dimensional (1D) Rashba effect has become quite important due to its key role in basic science to realize exotic electronic phenomena, such as Majorana bound states. Similar to the two-dimensional or three dimensional systems, the modulation of Rashba effect in 1D matrix is the kernel of spintronics for manipulating electron spin. Herein, by investigating the effects of transverse and vertical external electric field (EEF) on the Rashba spin splitting and magnetic anisotropy energy (MAE) in a type of highly flexible 1D system (Gd-adsorbed zigzag graphene nanoribbons) from first principles, we found that the Rashba spin splitting in such 1D system can be effectively regulated by the transverse EEF. Moreover, perpendicular magnetic anisotropy holds with either transverse or vertical EEF applied, despite obvious modulation of the MAE contributions in k space as well as the Rashba spin splitting. The modulation mechanism is further analyzed from the orbital-decomposed band structures and spin density for Gd-zigzag graphene nanoribbons (ZGNRs) at different electric-field values. It is found the modulation of Gd $5d_{x^2-y^2}$, d_{xy} by C p_z orbitals of edge states is the key to manipulating the magnetic anisotropy, which even plays a decisive role in modifying the Rashba spin splitting in such 1D nanoribbon system. The MAE and 1D Rashba spin splitting are expected to be controlled through modifying the edge states in such systems via EEF or other means. Our study introduces a strategy to manipulate Rashba spin splitting by edge states and provides insight into the magnetic anisotropy in 1D Rashba system, which would revitalize further research in ZGNR-based systems within the spintronics and exotic electronic phenomena.

DOI: 10.1103/PhysRevB.101.014451

I. INTRODUCTION

Manipulating magnetism (such as magnetic anisotropy [1–4], magnetic exchange coupling [5], or Rashba spin split [6–9]) with various methods is the focus of ongoing extensive research in the field of spintronics. Among these methods, external electric field (EEF) controlling of magnetization attracts a great deal of attention for the potential applications in spintronics and is also a key challenge for designing quantum magnetic properties. There are many successful studies focusing on the modulation of magnetic anisotropy by applying EEF [1–3]. For instance, EEF can maximize or momentarily decrease the magnetic anisotropy energy (MAE) on the freestanding monolayer or substrate supported films [1,2], thereby stabilizing a magnetic bit for long-term storage or facilitating magnetization reversal when writing information [3]. The underlying mechanism is reported to be lying in the EEF modulated electronic structure that is determined by the second-order perturbation [10].

The Rashba spin split [11] in low-dimensional states have been studied extensively due to the potential applications in next-generation spintronics [12]. Especially, one-dimensional (1D) states are promising because of the downsizing of the system and the highly efficient suppression of backscattering. 1D Rashba spin-splitting states have attracted much attention in basic science research to realize exotic electronic phenomena such as Majorana bound states [13] and spin-dependent density-wave formation [14]. Moreover, 1D Rashba effect can overcome the limitations of the two-dimensional (2D) Rashba effect. A pure spin current using an external magnetic field is an example of the nature peculiar to the 1D Rashba effect [15]. In fact, it is a nondissipative spin current because the Fermi surface has unidimensional dispersion peculiar to 1D systems, which is an ideal feature for spintronic devices. Based on the above advantages, 1D Rashba effect becomes more important. Recently, the 1D Rashba effect has been successfully realized in pure heavy-metal (such as Bi [16], Au [17], and Pt [18]) nanowires or Bi-adsorbed In atomic chains [19], which are artificially grown on a silicon surface. Interestingly, the 1D

*qzz@zzu.edu.cn

†qin.phys@gmail.com

‡Present address: Shenzhen JL Computational Science and Applied Research Institute, Longhua District, Shenzhen 518110, China.

§xzuo@nankai.edu.cn

Rashba systems above also present a sizable *out-of-plane* spin polarization [16–19]. Up to now, controlling the Rashba spin splitting by EEF in solid is at the center of spintronics for manipulating the electron spin [6], which has been well studied for 2D [7–9] host systems, such as the Au(111) surface, the polar perovskite surfaces and interfaces, etc. The EEF tuned Rashba splitting in 2D systems can be realized by modifying the gradient of the surface electrostatic potential or by manipulating the 2D electron gas. However, the research on the manipulation of 1D Rashba spin splitting is still lacking in both the experimental and theoretical levels. The modulations of Rashba effect in 1D systems are expected to have a different behavior and mechanism compared to the 2D and three-dimensional systems, which deserve comprehensive studies.

On the other hand, previous studies pointed out that the electronic and magnetic properties of graphene are sensitive to EEF [20–22], and similar phenomena were also found for the graphene nanoribbon [23,24]. Nevertheless, the role of EEF on the magnetic properties of graphene nanoribbon adsorbed with magnetic impurity has been barely explored, which especially lacks fundamental understanding at the theoretical level. In previous work [25], we have predicted a Rashba spin splitting in one-dimensional Gd adsorbed zigzag graphene nanoribbons (ZGNRs), which uncovers fundamental physics in graphene nanoribbons. However, there still exist challenges that are necessary to be addressed for promoting its applications in spintronics: (i) What is the performance of such 1D Rashba systems under an EEF? (ii) Can the Rashba spin splitting in such 1D Rashba systems be effectively manipulated by applying EEF? (iii) What is the mechanism underlying the EEF manipulation of the magnetic properties of 1D Rashba systems? The answers to the three questions are keys to the effective manipulation of magnetism of 1D Rashba systems by applying EEF, which would be helpful for guiding the experiments to design such tunable Rashba systems via EEF.

Motivated by the challenges, herein we study the effect of EEF on the magnetic anisotropy and Rashba spin splitting of Gd-ZGNR, where the transverse (E_y) and vertical (E_z) EEFs are considered, respectively. It is found that the perpendicular magnetic anisotropy (PMA) is maintained with either E_y or E_z applied. The values of MAE range from 0.85/0.9 to 4.36/3.44 meV under E_y/E_z, respectively. Based on the orbital-decomposed band structures, the MAE contributions along k line with EEFs applied are comprehensively discussed by isolating the first-order part originated from Rashba effect and second-order part, respectively. Furthermore, it is more important to identify that MAE contributions along k line as well as Rashba spin splitting can be effectively modulated by changing the coupling between Gd $-$ $5d_{x^2-y^2}$ and d_{xy} orbitals near E_f with applied transverse EEF, which both are driven by edge states basically. This work comprehensively clarifies the underlying mechanism of the tunable Rashba spin splitting and persisting perpendicular magnetic anisotropy in such 1D nanoribbon systems with external electric fields.

II. COMPUTATIONAL DETAILS

Density-functional theory calculations are performed using the projected augmented wave (PAW) [26] method as implemented in the Vienna *Ab initio* Simulation Package (VASP) [27]. Exchange-correlation energy functional is treated in the Perdew-Burke-Ernzerhof of generalized gradient approximation (GGA) [28]. The valence electron configurations of Gd are considered as $4f^7 5d^1 6s^2$. The wave functions are expanded in plane-wave basis with a kinetic energy cutoff of 450 eV. The partially filled and strongly correlated localized f orbitals of Gd atoms are treated using the GGA+U formalism [29,30] with $U_f = 8$ eV [31]. In this work, we focus on the response of magnetic properties of Gd adsorbed ZGNR to the EEF, which is introduced by planar dipole layer method [32] as implemented in VASP. Both the EEF along y (E_y) and z (E_z) axis are considered in our calculations, respectively. Specifically, the E_y/E_z are applied to the stable $h_1 - \mathrm{Gd} - \mathrm{ZGNR}$, respectively, in the range of $-0.8\,\mathrm{V/Å} \leqslant E_{y/z} \leqslant 0.8\,\mathrm{V/Å}$. The directions of EEF are defined as stated below (inset of Fig. 1). The dipole correction [33] is included to avoid the interaction between period crystals.

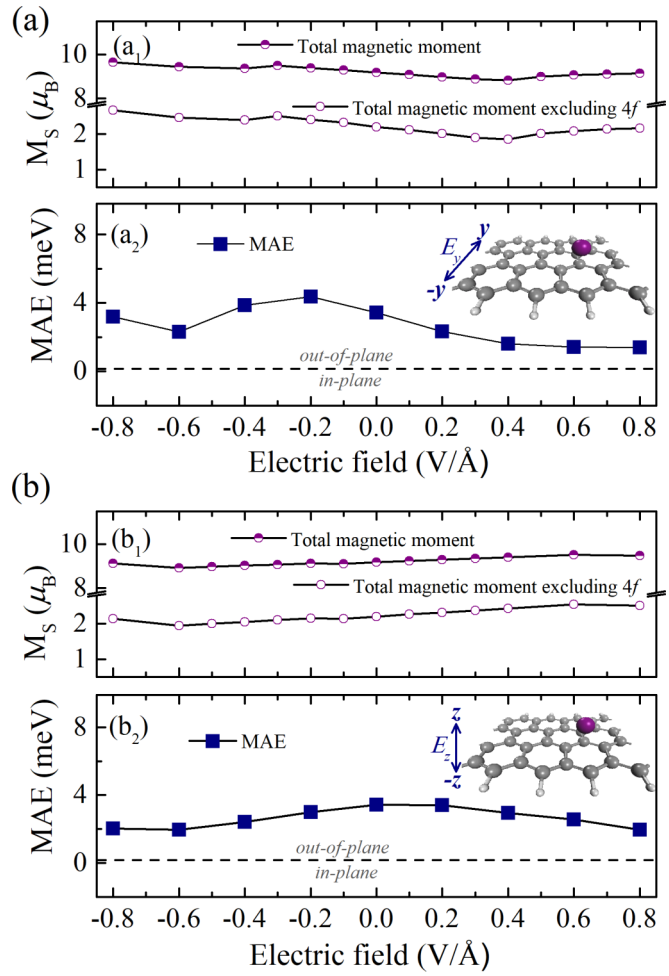

FIG. 1. (a) The magnetic moment (a_1) and MAE (a_2) of Gd-ZGNR with E_y applied. The E_y is parallel with the nanoribbon plane but perpendicular with the edges of nanoribbon as shown in the inset figure. (b) Similar with (a), but the EEF is applied along the z direction (E_z). The E_z is perpendicular with the plane of nanoribbon. Positive and negative MAE represent the out-of-plane and in-plane magnetization, respectively.

Previous study concluded that the adsorption position and magnetic anisotropy contributions in k space do not change

substantially with the increase of nanoribbon width [25], which indicates that the ZGNR with width of 4 unit cells ($N = 4$) is wide enough to study the magnetic properties and Rashba effect of Gd-ZGNRs. Here we adopt the calculated model with width $N = 4$ of ZGNR with a Gd atom adsorbed, where the x direction along the Gd-ZGNR nanoribbon is treated as periodic and infinite (inset of Fig. 1), and the vacuum thicknesses along the y and z direction are set as 20 and 15 Å, respectively. Prior to studying the magnetic properties of Gd-ZGNR with EEF applied, we first optimized the geometry structures under different EEF strengths to study the effect of EEF on the structural characteristics of Gd-ZGNR. Brillouin zones (BZs) are sampled using $15 \times 1 \times 1$ Monkhorst-Pack grids for the geometry optimization for all EEF values. In the optimization process under EEF, the Gd adatom is allowed to relax along the z direction and all the C atoms are allowed to relax along all directions, until the force on each atom is less than 0.03 eV/Å. The convergence criterion of the self-consistent-field (SCF) calculations is 10^{-6} eV. In the self-consistent potential and total energy calculations, a set of $25 \times 1 \times 1$ k-point sampling is used for BZ integration. For band-structure calculations, 60 uniform k points along the Γ-M are used. Considering the spin-orbit coupling (SOC) term, the MAE can be calculated as the energy difference following the Force theorem [34] $E_{\mathrm{MAE}} = E_{[100]} - E_{[001]}$, where $E_{[100]}$ and $E_{[001]}$ are the total energy for the magnetization oriented along the parallel [100] and perpendicular [001] directions, respectively. In addition, we also checked the total energy for the magnetization oriented along the parallel [010] and it is almost equivalent to that along the [100] direction, which is obviously higher than that along the [001] direction (see the Supplemental Material [35]). Therefore, the magnetization direction of [010] is not considered [25]. Here, the [100], [010], and [001] directions are corresponding to the x, y, z, axis, respectively.

III. RESULTS AND DISCUSSION

Before we comprehensively studied the magnetic properties of Gd-ZGNR with applying EEFs, we first check the effect of EEF ($-0.8\,\mathrm{V/Å} \leqslant E_{y/z} \leqslant 0.8\,\mathrm{V/Å}$) on the geometry structure of Gd-ZGNR (Fig. S1 of Supplemental Material [35]). It is found that the EEFs have a minor impact on the position of Gd adatom, especially for the horizontal distance between Gd atom and the left-edge C atom d_{hor}, indicating the stable adsorption of Gd atom on the hollow site. In contrast, the change of the average vertical distance between Gd atom and ZGNR plane (d_{ver}) is relatively remarkable, especially for the E_z and positive E_y which induce sinking of the Gd adatom. For $E_y = 0.8\,\mathrm{V/Å}$, d_{ver} is changed from 2.14 to 2.06 Å. For $E_z = -0.8$ and 0.8 V/Å, d_{ver} changes to 2.08 and 2.09 Å, respectively. With EEF (E_y or E_z) applied in the range from -0.8 to 0.8 V/Å, the maximum variations of d_{ver} and d_{hor} are ∼0.058 and ∼0.016 Å, respectively. In view of the fact that the EEFs cause changes to the geometry structure, we subsequently studied the physical properties of Gd-ZGNR with applied EEF based on the optimized structures.

A. Magnetic moment and perpendicular magnetic anisotropy

Based on the optimized geometry structures, we explore the magnetic moment and MAE of the Gd-ZGNR system with EEF ($-0.8\,\mathrm{V/Å} \leqslant E_{y/z} \leqslant 0.8\,\mathrm{V/Å}$) applied. The total magnetic moment of Gd-ZGNR and that excluding the contribution of Gd $4f$ under E_y and E_z are shown in Figs. 1(a_1) and 1(b_1), respectively. The trends of the total magnetic moment with and without the contribution of Gd $4f$ are consistent with each other. The reason lies in the energetically stable half-filled f-electron configuration, which plays a negligible role in the changes of magnetic moment under EEF. We focus on the analysis of total magnetic moments excluding the f-orbital contribution in the following. In Figs. 1(a_1) and 1(b_1), the magnetic moment of Gd-ZGNR at $-0.8\,\mathrm{V/Å} \leqslant E_y \leqslant 0.8\,\mathrm{V/Å}$ varies from 1.85 to 2.67 μ_{B} at E_z, while it changes from 1.89 to 2.54 μ_{B} at E_y. The changes in magnetic moment are mainly dominated by the hybridization between Gd and the neighboring C atoms which changes with the applied E_y or E_z. The nature of the EEF modulated magnetic moment can be reflected by the shift of Fermi level from the perspective of electronic structures. Note that, whether in the case of E_y or E_z, the spin density of two edge states of ZGNR plane maintains the asymmetric antiferromagnetic coupling.

To study the effect of EEF on magnetic anisotropy of Gd-ZGNR, we further calculate the MAE of Gd-ZGNR with E_y and E_z applied, respectively. The MAE is defined as the energy eigenvalue difference ($E_{\mathrm{MAE}} = E_{[100]} - E_{[001]}$) for the magnetization oriented along the *in-plane* [100] and *out-of-plane* [001] directions, respectively. The E_{MAE} for pristine Gd-ZGNR (without EEF) has a positive value of 3.44 meV. With EEF applied, it is found that E_{MAE} can be effectively modulated in the range of ([0.85, 4.36] meV at E_y and [0.9, 3.44] meV at E_z) under $-0.8\,\mathrm{V/Å} \leqslant E_{y/z} \leqslant 0.8\,\mathrm{V/Å}$ [Figs. 1(a_2) and 1(b_2)]. The E_{MAE} always maintains positive sign, which means that the energetically favorable direction for the magnetization remains the out-of-plane [001] direction regardless of E_y or E_z applied [Figs. 1(a_2) and 1(b_2)]. The robust out-of-plane magnetization indicates that Gd-ZGNR is expected as an excellent candidate for vertical magnetic anisotropy magnetic random-access memory [36].

The results of MAE are different from that of non-Rashba systems [3,37–39] where the sign of MAE (magnetization direction) in the Rashba system can be switched between negative (in-plane) and positive (out-of-plane) [3,37,38], or presents in-plane magnetization [3] under a wide range of EEF. The robust out-of-plane magnetization of Gd-ZGNR under EEF may originate from the 1D Rashba nature. The coexistence of PMA and Rashba has been discussed in previous studies [16,17,40,41]. In particular, it has been reported that many Rashba systems, regardless of whether they are 2D [40,41] or 1D systems [16,17], show a finite out-of-plane spin polarization. The out-of-plane spin polarizations are also possible in 1D systems because they usually show lower in-plane symmetry. The calculated PMA further demonstrated that the out-of-plane magnetization maintains in such 1D Rashba system. To achieve a fundamental understanding on the persistent magnetic anisotropy in the Gd-ZGNR system, the evolution of MAE contributions at each k point with EEF applied will be discussed from the view of orbital-resolved band structures and edge spin density.

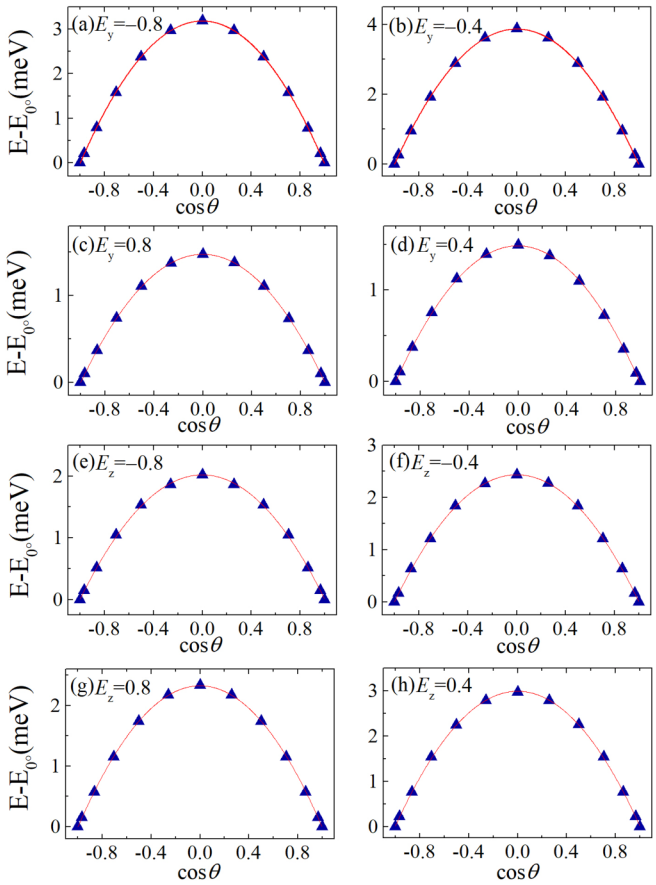

FIG. 2. Angle (θ)-dependent MAE of Gd-ZGNR with EEF applied. (a)–(d) $E_y = -0.8$, -0.4, 0.4, 0.8 V/Å. (e)–(h) $E_z = -0.8$, -0.4, 0.4, 0.8 V/Å. The angle θ ($0° \leqslant \theta \leqslant 180°$) is defined as the angle between z axis and spin direction. Blue triangular line represents the calculated data and red solid line represents fitting curve.

B. Magnetic anisotropy and Rashba spin splitting

The changes in MAE values rely on the charge transfer of the system, which leads to the shift of E_f and then alters the orbitals contributions. Thus, the sign and value of MAE at each k line are finally determined. To get a deep understanding on the EEF modulated MAE of Gd-ZGNR in Figs. 1(a_2) and 1(b_2), we studied the angle-dependent MAE and MAE contributions in k space under EEF.

1. Angle-dependent MAE

Firstly, the angular (θ)-dependent MAE at $0° \leqslant \theta \leqslant 180°$ is calculated and the angle dependence of MAE on cosθ is fitted to $E_{\mathrm{MAE}} = K_0 + K_1\cos\theta + K_2\sin^2\theta$ at $E_{y/z}$ (-0.8, -0.4, 0.4, 0.8 V/Å), respectively, as shown in Figs. 2(a)–2(h). Angle θ is defined as the angle between the quantization axis of spin and the vertical z axis. The angle-dependent MAE is fitted into the second-order polynomial of cosθ, the coefficients of which quantify the perturbations at different orders. The parabolic curves and the fitted coefficients of the polynomial fitting formula ($K_0 + K_1\cos\theta + K_2\sin^2\theta$) are plotted in Figs. 2(a)–2(h) and summarized in Table I, respectively. The coefficients K_1 and K_2 are associated with the first- and second-order perturbations, respectively. The standard errors for all fitted coefficients are small and acceptable. All fitted coefficients K_1 are close to zero in Table I and the leading term of the calculated MAE is proportional to $\sin^2\theta$, which confirms the theoretical predictions that the first-order perturbation of intrinsic SOC ($\mathbf{L}\cdot\mathbf{S}$ term) has no contribution to MAE as well as the Rashba SOC term [42,43]. In addition, it is shown by the polynomial fitting that it is sufficient to illustrate the calculated MAE contributions in k space of Gd-ZGNR in the external electric field E_y or E_z in terms of the second-order perturbation [10].

TABLE I. The fitted values of MAE of Gd-ZGNR under EEF based on polynomial fitting formula ($K_0 + K_1\cos\theta + K_2\sin^2\theta$), which are corresponding to the fitted curves in Fig. 2 of text. For the case of $E_{y/z} = -0.8$, -0.4, 0.4, 0.8 and V/Å, the K_0, K_1, K_2 and the respective standard errors are presented.

Electric field	$K_0 + K_1\cos\theta + K_2\sin^2\theta$	Standard error
$E_y = -0.8$	$K_0 = 3.179$ $K_1 = -5 \times 10^{-4}$ $K_2 = 3.187$	$A = 0.004$ $B_1 = 0.003$ $B_2 = 0.006$
$E_y = -0.4$	$K_0 = 3.862$ $K_1 = 2 \times 10^{-4}$ $K_2 = 3.872$	$A = 0.005$ $B_1 = 0.004$ $B_2 = 0.008$
$E_y = 0.4$	$K_0 = 1.485$ $K_1 = -0.009$ $K_2 = 1.487$	$A = 0.004$ $B_1 = 0.003$ $B_2 = 0.005$
$E_y = 0.8$	$K_0 = 1.475$ $K_1 = -1 \times 10^{-4}$ $K_2 = 1.474$	$A = 0.003$ $B_1 = 0.002$ $B_2 = 0.005$
$E_z = -0.8$	$K_0 = 2.022$ $K_1 = -9 \times 10^{-5}$ $K_2 = 1.996$	$A = 0.009$ $B_1 = 0.007$ $B_2 = 0.010$
$E_z = -0.4$	$K_0 = 2.435$ $K_1 = 5 \times 10^{-5}$ $K_2 = 2.396$	$A = 0.005$ $B_1 = 0.004$ $B_2 = 0.008$
$E_z = 0.4$	$K_0 = 2.989$ $K_1 = 3 \times 10^{-4}$ $K_2 = 2.972$	$A = 0.009$ $B_1 = 0.007$ $B_2 = 0.014$
$E_z = 0.8$	$K_0 = 2.324$ $K_1 = 1 \times 10^{-4}$ $K_2 = 2.329$	$A = 0.002$ $B_1 = 0.002$ $B_2 = 0.004$

2. MAE *contributions in the k space and Rashba spin splitting*

Although the first- and second-order MAE contributions both come from intrinsic and Rashba SOC in a finite electric field, the first-order contribution, not like the second-order part, vanishes as the fitted coefficient K_1 is close to zero, and can only be traced in the MAE distribution of k space. The underlying mechanism is that the Rashba spin splitting could manipulate the electron trajectory determined by the spin direction in the k space, and consequently creates a counterbalanced first-order MAE part in the first Brillouin zone (FBZ). Here, to examine the role of EEF on the first-order MAE as well as Rashba spin split in Gd-ZGNR, we first calculate the total MAE contributions in k space according

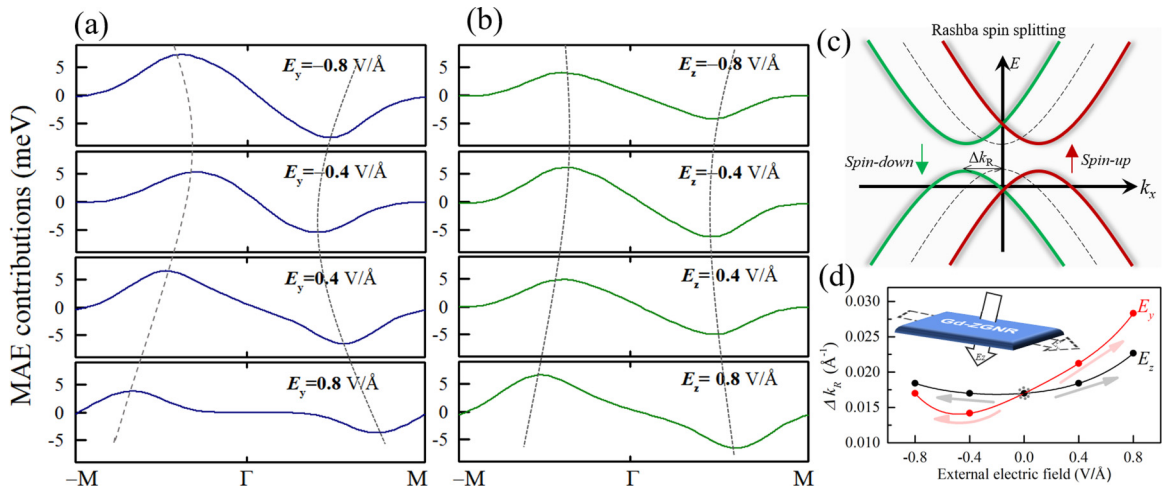

FIG. 3. The MAE contributions in FBZ ($-M$-Γ-M) calculated by $E_{100} - E_{001}$ of Gd-ZGNR with (a) E_y and (b) E_z ($E_{y/z} = -0.8, -0.4, 0.4, 0.8$ V/Å) applied, respectively. (c) Schematic diagram of Rashba spin splitting under EEF. The moment splitting Δk_R is defined as the horizon shift. (d) The Δk_R as a function of $E_{y/z}$, where different directions are labeled by red and black solid circles, respectively.

to the formula below:

$$\Delta E(\vec{k}) = E_a(\vec{k}) - E_b(\vec{k}) = \sum_{k \in FBZ} \left(\sum_{i \in o} \varepsilon_i^a(\vec{k}) - \sum_{i \in o'} \varepsilon_i^b(\vec{k}) \right), \tag{1}$$

where the $\varepsilon_i^a(\vec{k})$ and $\varepsilon_i^b(\vec{k})$ is the energy of the ith band at point k in the FBZ for the magnetic states with spin moments aligned on the directions of a and b, respectively. The o and o' specify the occupied states for the a and b directions, respectively. Note that the curve trend of MAE contributions in k space can be used to understand how the EEF affects the Rashba spin splitting.

Figures 3(a) and 3(b) show the MAE contributions in k space under an EEF of E_y and E_z (-0.8, -0.4, 0.4, 0.8 V/Å), respectively. The maximum energy of MAE in $-M \sim \Gamma$ is fluctuating in the range of 3.8∼7.3 meV under E_y, while for the E_z, the energy peak varies between 4.1 and 6.5 meV. Specially, the MAE contribution in k space of Gd-ZGNR system under $E_{y/z}$ still has a Γ-centered offset trend in FBZ, and EEF can affect the first-order effect as well as Rashba spin splitting. Compared with MAE behavior of Gd-ZGNR under E_z [Fig. 3(b)], the splitting amplitude of MAE in the k space at E_y [Fig. 3(a)] is more obvious. The mechanism underlying these changes is that the Fermi level in band structure moves under EEF, causing further changes of the occupied state in the k space. Figure 3(d) shows the changes of amplitude of Rashba spin splitting (Δk_R) at EEF, which is defined in Fig. 3(c). It is found that the transverse EEF can significantly increase Δk_R at positive values, and Δk_R can be largely reduced at a certain negative value ($E_y \geqslant -0.4$ V/Å). Compared with Δk_R at E_z, E_y can manipulate the Δk_R more obviously, which indicates that the outward EEF (E_y) can effectively regulate the spin-splitting moment of the Rashba system Gd-ZGNR.

3. *First-order and second-order* MAE *contributions*

To clarify the origin of EEF modulated MAE in Figs. 1(a_2) and 1(b_2), we need to isolate the first-order part of MAE contributions over the whole Brillouin zone from the pure second-order part. First, we can obtain the MAE contribution of the first order from the formula $E = K_0 + K_1 \cos\theta + K_2 \sin^2\theta$. It is inferred that there is no second-order contribution in the difference between the MAEs calculated for the spin along z and –z directions. Thus, based on the formula $\Delta E'(\vec{k}) = E_{-z}(\vec{k}) - E_z(\vec{k}) = \sum_{k \in FBZ} (\sum_{i \in o} \varepsilon_i^{-z}(\vec{k}) - \sum_{i \in o'} \varepsilon_i^z(\vec{k}))$, the first-order MAE contribution in k space can be obtained directly, that is $\Delta E'/2$. Furthermore, by subtracting the first-order MAE contribution from the total contribution of the MAE in k space ($\Delta E = E_{(100)} - E_{(001)}$), we can further obtained the pure second-order part of MAE contributions in k space of Gd-ZGNR, which essentially leads to the change in MAE values.

Figure 4 shows the first-order ($\Delta E'/2$) (the upper part) and second-order MAE contributions (the lower part) in k space of Gd-ZGNR at $E_{y/z}$ = (a, e) −0.8 V/Å, (b, f) −0.4 V/Å, (c, g) 0.4 V/Å, and (d, h) 0.8 V/Å. The results show that the distributions of first-order MAE contribution are exactly antisymmetric about the Γ point, like that of Gd-ZGNR without an external electric field, which leads to the perfect cancellation of the MAE distribution over the first Brillouin zone, as indicated by $K_1 = 0$ in the results of polynomial fitting.

We subtract the part of first-order contribution from total contributions along k line; the pure second-order MAE contributions along Γ-M with different EEFs are obtained, as shown in the top of Fig. 5, which can be analyzed by the second-order perturbation theory [10]. The formula is expressed as

$$\Delta E \sim \sum_{u,o} \frac{|\langle u|l_z|o\rangle|^2 - |\langle u|l_x|o\rangle|^2}{\varepsilon_u - \varepsilon_o}, \tag{2}$$

where u and o specify the unoccupied and occupied minority spin states, respectively, and the l_x and l_z are angular momentum operators. The pair of unoccupied and occupied states around Fermi level is important to the second-order MAE contribution. As pointed out previously, $\Delta E_{\downarrow\downarrow}$ only contributes a small amount to MAE near the M point, and the MAE contribution in k space mainly comes from

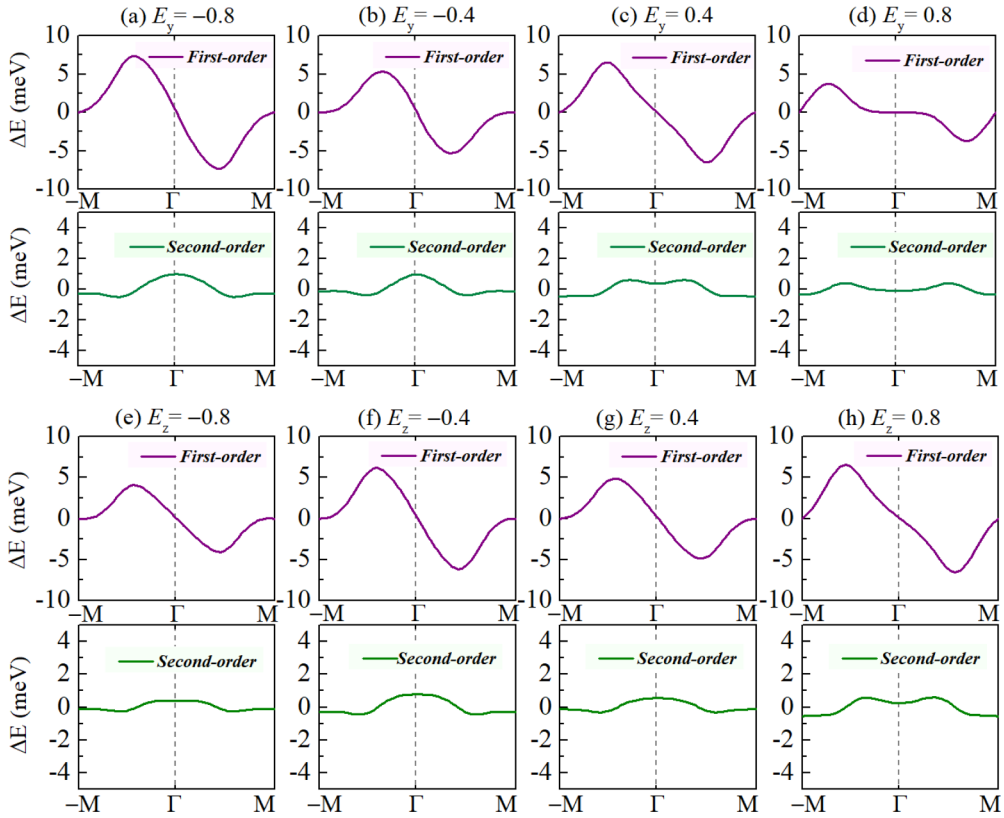

FIG. 4. The first- and second-order part of MAE contributions in FBZ ($-M$-Γ-M) of Gd-ZGNR applied with $E_{y/z}$ = (a, e) −0.8 V/Å, (b, f) −0.4 V/Å, (c, g) 0.4 V/Å, and (d, h) 0.8 V/Å.

$\Delta E_{\uparrow\uparrow}$ [25]. Therefore, the MAE contribution under EEF can be analyzed based on the coupling between the spin-up electronic states ($\Delta E_{\uparrow\uparrow}$) as follows. Taking $E_{y/z} = -0.4, 0.4$ V/Å as examples, the orbital-projected band structure with the Gd spin-up orbital occupied probability and the spin-up/down orbital contribution of C p_z are provided in the middle and lower part of Fig. 5, respectively. For better comparison, the orbital-projected band structure without EEF is also provided in Fig. 5(b). Without EEF applied, $d_{x^2-y^2}$ and d_{z^2} orbitals located above and below E_F; d_{xz} orbital is located above E_F except near M; the whole d_{xy} orbital located above E_F, whose orbitals lie in the layer plane with $d_{x^2-y^2}$, and form the near-degenerate state with $d_{x^2-y^2}$ at Γ.

Based on the perturbation theory in Eq. (1) [10], the SOC between occupied and unoccupied states with the same (different) magnetic quantum number m through the $L_z(L_{x/y})$ operator gives a positive (negative) contribution to the E_{MAE}. As seen from Fig. 5(b), the SOC interaction between the occupied $d_{x^2-y^2}$ ($m = \pm 1$) state at −1.05 eV and the unoccupied d_{xy} ($m = \pm 1$) state at 0.2 eV around Γ through the l_z operator ($\langle d_{xy}|l_z|d_{x^2-y^2}\rangle$) yields a positive E_{MAE} at ∼2/5 Γ-M. At Γ, the SOC interaction of near-degenerate states $d_{x^2-y^2}$ (d_{xy}) at 0.2 eV also makes for a positive E_{MAE}, whereas the coupling of $\langle d_{xz}(d_{x^2-y^2})|l_x|d_{x^2-y^2}(d_{xz})\rangle$ contributing negatively to MAE range from −0.3 to 0.6 eV at the second half (∼3/5 Γ-M), corresponding to the second part of Eq. (2).

When the EEF is introduced, the band structures move up and down compared to that in zero field as shown in Fig. 5. Especially, a significant difference is observed near the regions around E_f, e.g., at $E_y = 0.4$ V/Å [Fig. 5(c)]. The degenerate state of two bands 1 and 2 at Γ above E_f becomes more obvious, which are pushed up above E_f together by the EEF, leading to the hybridization of bands 2 and 3 with each other at 4/5 Γ-M. Thus, the lifting of bands makes the unoccupied d_{xy} orbital of band 2 coupled to the unoccupied $d_{x^2-y^2}$ state at 0.82 eV through the l_z operator ($\langle d_{xy}|l_z|d_{x^2-y^2}\rangle$) at ∼1/2 Γ-$M$, leading to an expansion of positive E_{MAE} in k line. The positive E_{MAE} at Γ is reduced because of the degenerate states $d_{x^2-y^2}$ (d_{xy}) of bands 1 and 2 are pushed away above E_f 0.35 e V by the positive EEF. On the contrary, at $E_y = -0.4$ V/Å [Fig. 5(a)], bands 1 and 2 are pushed down close to E_f by the EEF and promote a splitting of the degenerate energy states at Γ. The intersection point of band 1 with E_f is getting closer to Γ due to the band structure moving down, which leads to the narrowing of positive E_{MAE}, and naturally expanded the negative E_{MAE} in k line because of the occupied $d_{x^2-y^2}$ orbital of band 1 coupling with unoccupied d_{xz} of band 3. In short, the percentage of positive or negative E_{MAE} in k line is mainly dominated by the SOC coupling between d_{xy} and $d_{x^2-y^2}$ orbitals.

The situation is similar for the cases with E_z applied, but the overall band structure shifted enormously compared to the cases at E_y. The movement of intersection point of band 1 with E_f is less obvious as shown in Figs. 5(d) and 5(e). Thus, there are not too many changes of E_{MAE} in k line. The trend of moving up of band 1 and 2 at $E_z = -0.4$ V/Å is similar but not obvious compared to that at $E_y = 0.4$ V/Å. In short, the location of E_f adjusts the components of different types of

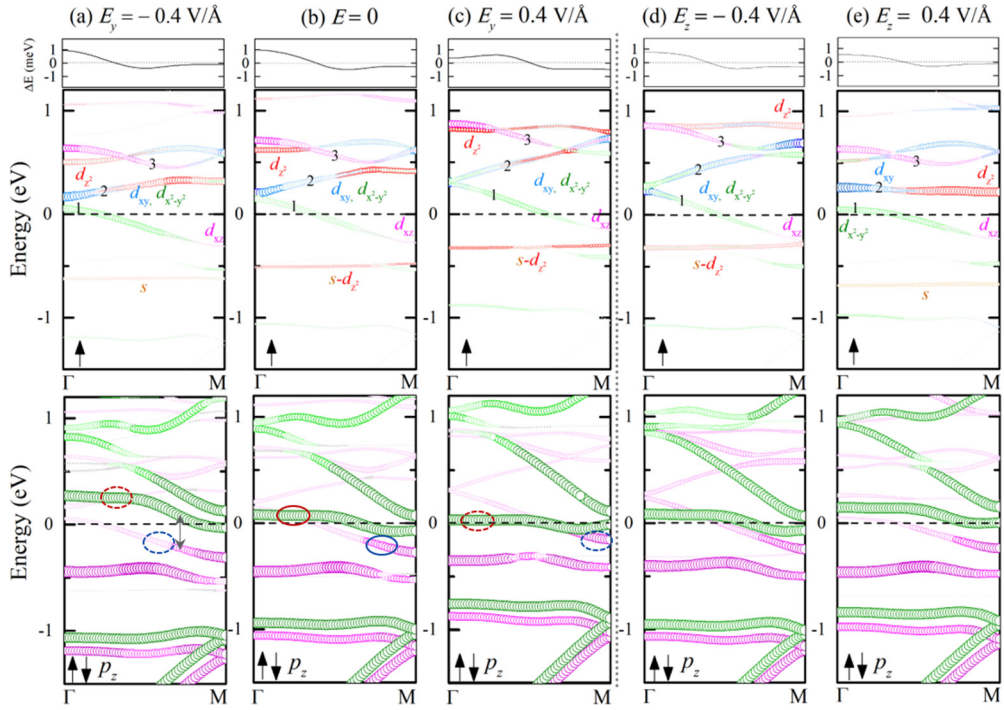

FIG. 5. The second-order MAE contributions along Γ∼M and the orbital-projected band structures (Gd − sd spin-up states and C − p_z spin-up/down states) of Gd-ZGNR (b) without applying an EEF, with applying the E_y in value of (a) −0.4 V/Å and (c) 0.4 V/Å, and E_z in value of (d) −0.4 V/Å and (e) 0.4 V/Å. The orange, blue, green, rose, and red colors represent the occupation of Gd-s, d_{xy}, $d_{x^2-y^2}$, d_{xz}, d_{yz} and d_{z^2} orbitals, respectively. The C − p_z spin-up/down states in the lower part are indicated by the rose/green circle, respectively. The size of color circles measures the occupied proportion of each orbital. The red and blue circles are labeled in the C − p_z orbital part to better show the relative shift of band 1 and band-down 1 around E_f.

orbital contributions, which is crucial for the determination of the symbol and size of MAE in each segment of k space.

4. The role of edge states

As observed in the lower part of Fig. 5, the second half of band 1 (∼2/5 M-Γ) is composed of p_z spin-up states, which is together manipulated with the $d_{x^2-y^2}$ orbital of bands 1 by the EEF, especially at E_y. In the view of charge distribution in real space, the spin-up/down states of p_z orbital at two edge states of ZGNR transfer from one side to another side with a transverse EEF (E_y) applied. Thus, the relative locations of E_f in the spin-up and spin-down electronic structures are changed, which thereby change the orbital hybridization in Gd-ZGNR. Next, we further intuitively clarify the behavior of the edge states when EEF is introduced. To focus on the changes of edge states, we calculated the difference between spin densities $\Delta\rho = \rho_{E_{y/z}} - \rho_{E_0}$ (subtracting the spin density without electric field from that of the system with applied electric field) derived from Fig. S3 of the Supplemental Material [35].

The 2D spin-density differences across the ZGNR plane are plotted in Fig. 6(a). As revealed by the $\rho_{E_y} - \rho_{E_0}$, the response of spin density to E_y is obviously much stronger compared to that with E_z field applied. Therefore, we mainly focus on the changes at E_y in the following analysis. Note that the spin-up density is considered as a positive value in spin-density data and the spin-down density is a negative value. Thus, we use the signs "+" and "−" in E_0 to mark their locations, which helps to make a clear understanding of the changes of spin density. When the subtraction of the spin-density data between E_y and E_0 is carried out, the subtraction results of spin-up (+) densities directly represent gain or loss electrons, as revealed in the color bar of Fig. 6(a), whereas the subtraction results of spin-down (−) densities mean the opposite, and it should be considered as in contrast to the intuitive results of + spin densities. For the nonspecific positive E_y, e.g., $E_{y=0.4} - E_0$, the spin density at left edge (SPL) increased and spin density of edge states at right side (SPR) decreased, which led to the characteristic of the original asymmetric spin-density alleviate. On the contrary, the SPR is increased and SPL is decreased at the negative E_y, further exacerbating the characteristic of original asymmetric of edge states in Gd-ZGNR. It should be pointed out that, with E_y applied, the response of two edge states is quite different from that of pure ZGNR with E_y applied [24]. In the case of pure ZGNR, spin electrons of edge state on one side transfer to another side. The spin-up and spin-down density will counteract on the receiver, thus leading to the simultaneously degenerated spin density at both two edge states [Fig. 6(c)]. However, for the case of Gd-ZGNR at E_y, the process is totally different. For instance, at $E_y = 0.4$ V/Å, when spin-up electrons at the right side transfer to the left side consisting of spin-down electrons, there is a positive contribution to the SPL as RPL decreased. This is because the spin flip appears during the transfer process due to the spin modulation of Gd, as revealed in the sketch map of Fig. 6(b). The mechanism is similar for that with E_y applied along the opposite direction. Spin flip

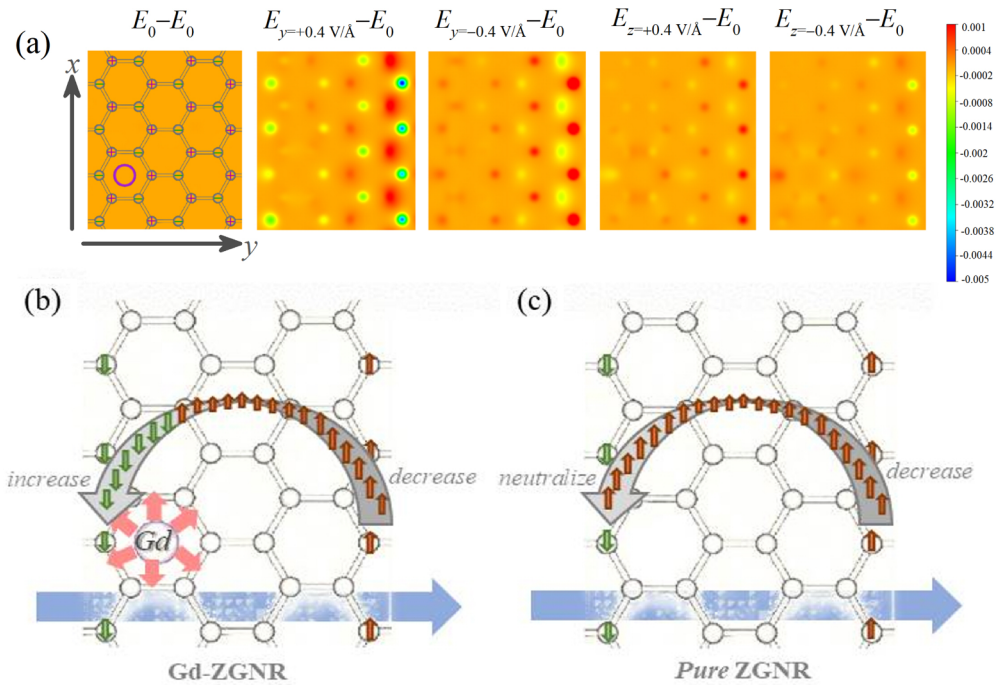

FIG. 6. (a) The differences between spin densities $\Delta\rho = \rho_{E_{y/z}} - \rho_{E_0}$ for the ZGNR plane of system without and with EEF. The atom location in the ZGNR plane is provided for an intuitive comparison with other cases. The color bar is given in the units of $e/\text{Å}^3$ (the red regions indicate gain electrons; the blue regions indicate lost electrons). In the left subfigure of (a), the green "−" represent the location of spin-down states, while red "+" represent the location of spin-up states. (b), (c) Schematic diagrams of spin charge transfer in Gd-ZGNR and pure ZGNR. In pure system with EEF applied (c), the spin-up electrons moved from one side to another side and further neutralized the spin-down electrons at the other side, leading the degradation of two edge states. While in Gd-ZGNR (b), the situation is changed due to existence of Gd.

happens in the electron transfer process, and the asymmetric edge states are consequently exacerbated.

Observed from the decomposed $C-p_z$ spin-up/down states in the lower half of Fig. 5, there are two bands crossing around E_f: The *band 1* mostly contributed by spin-down p_z (signed in Gd-*d* orbitals) and another band mainly contributed by spin-down p_z (we call it "*band down-1*"), which is labeled by red and blue circles, respectively. When $E_y = 0.4\,\text{V/Å}$ is introduced, the *band down-1* with spin-down p_z orbitals (green) moves down and the *band 1* with spin-up p_z (red) moves up relative to E_f. Thus, the electrons in *spin-up* states decrease, while the electrons in *spin-down* states increase, which is well consistent with the variation of edge spin states in Fig. 6(a). Conversely, at $E_y = -0.4\,\text{V/Å}$, the band down-1 with spin-down p_z orbitals (green) moves up and the band 1 with spin-up p_z (red) moves down near E_f, indicating the electrons in *spin-down* states reduced but increased in *spin-up* states. With the fact that the changes of MAE contribution in *k*-space controlled PMA is mostly dominated by the shift of band 1, it can be inferred that the changes of electrons at the two edge states are crucial to promoting the changes of $\text{Gd}-5d_{x^2-y^2}, d_{xy}$ orbital hybridization, and thus modify and determine the MAE contributions along *k* line. On the other hand, the counterbalanced MAE in *k* space as well as the Rashba effect are mainly originated from the movement of band 1 evidenced in Ref. [25], which indicates that the modulation of Rashba spin splitting is also driven by the changes of edge states under EEF. In short, the modulation of $\text{Gd}-5d_{x^2-y^2}, d_{xy}$ by $C-p_z$ orbitals of edge states is the underlying mechanism of the manipulation of the magnetic properties of Gd-ZGNR by EEF, which even plays a key role in the Rashba spin splitting of such 1D system.

IV. CONCLUSIONS

In summary, we have performed a systematic study on the role of EEF in the modulation of magnetic moment, MAE, Rashba spin splitting, and edge spin density of Gd adsorbed ZGNR. It is found that the response to transverse EEF is particularly remarkable as compared to vertical EEF. By isolating the first-order MAE contribution in *k* space due to Rashba spin split, the net second-order MAE contribution in *k* space is obtained and further analyzed by applying the traditional second-order perturbation theory to the orbital-decomposed band structures in an external electric field, where the MAE value is modified through changes in the coupling of $\text{Gd}-5d_{x^2-y^2}$ and d_{xy} orbitals near E_f. Furthermore, by exploring the spin-density difference of edge states when EEF is introduced, it is inferred that the modulation of $\text{Gd}-5d_{x^2-y^2}, d_{xy}$ by $C-p_z$ orbitals owing to the charge transfer between two edge states is not only the most essential reason of regulating MAE contributions in *k* space, but also the determinant of how the Rashba spin splitting changes under EEF.

Our findings of the modulation of $\text{Gd}-5d_{x^2-y^2}, d_{xy}$ by $C-p_z$ orbitals of edge states explain the nature of magnetic properties of the 1D Rashba system, especially for the response to EEF. The fundamental understanding is expected to shed light on the control of the MAE and further the Rashba spin splitting by changing the edge spin states in more possible manners beyond EEF. Our studies could lead

to promising applications of ZGNR in spintronics, which are expected to revitalize further research in 1D Rashba systems and its exotic electronic phenomena.

ACKNOWLEDGMENTS

This research is supported by the National Natural Science Foundation of China (Grants No. 11847158 and No. 11904324), Science Challenge Project (Grant No. TZ2016003-1-105), and the China Postdoctoral Science Foundation (Grant No. 2018M642774). G.Q. is supported by an ASPIRE grant from the Office of the Vice President for Research at the University of South Carolina, USA. The numerical calculations in this paper have been partly done on the supercomputing system of the National Supercomputing Center in Changsha.

[1] M. Tsujikawa and T. Oda, Finite Electric Field Effects in the Large Perpendicular Magnetic Anisotropy Surface Pt/Fe/Pt(001): A First-Principles Study, Phys. Rev. Lett. **102**, 247203 (2009).

[2] M. Weisheit, S. Fähler, A. Marty *et al.*, Electric field-induced modification of magnetism in thin-film ferromagnets, Science **315**, 349 (2007).

[3] A. Sonntag, J. Hermenau, A. Schlenhoff, J. Friedlein, S. Krause, and R. Wiesendanger, Electric-Field-Induced Magnetic Anisotropy in a Nanomagnet Investigated on the Atomic Scale, Phys. Rev. Lett. **112**, 017204 (2014).

[4] H. Chen, M. Song, Z. Guo *et al.*, Highly secure physically unclonable cryptographic primitives based on interfacial magnetic anisotropy, Nano Lett. **18**, 7211 (2018).

[5] K. L. Seyler, D. Zhong, B. Huang *et al.*, Valley manipulation by optically tuning the magnetic proximity effect in WSe_2/CrI_3 heterostructures, Nano Lett. **18**, 3823 (2018).

[6] R. Winkler, *Spin-Orbit Effects in Two-Dimensional Electron and Hole Systems* (Springer, New York, 2003).

[7] S.-J. Gong, C.-G. Duan, Y. Zhu, Z.-Q. Zhu, and J.-H. Chu, Controlling Rashba spin splitting in Au(111) surface states through electric field, Phys. Rev. B **87**, 035403 (2013).

[8] Q.-F. Yao, J. Cai, W.-Y. Tong, S.-J. Gong, J.-Q. Wang, X. Wan, C.-G. Duan, and J. H. Chu, Manipulation of the large Rashba spin splitting in polar two-dimensional transition-metal dichalcogenides, Phys. Rev. B **95**, 165401 (2017).

[9] K. V. Shanavas and S. Satpathy, Electric Field Tuning of the Rashba Effect in the Polar Perovskite Structures, Phys. Rev. Lett. **112**, 086802 (2014).

[10] D. Wang, R. Wu, and A. J. Freeman, First-principles theory of surface magnetocrystalline anisotropy and the diatomic-pair model, Phys. Rev. B **47**, 14932 (1993).

[11] E. I. Rashba, Properties of semiconductors with an extremum loop. I. Cyclotron and combinational resonance in a magnetic field perpendicular to the plane of the loop, Fiz. Tverd. Tela **2**, 1109 (1960) [Sov. Phys. Solid State **2**, 1224 (1960)].

[12] A. Manchon, H. C. Koo, J. Nitta, S. M. Frolov, and R. A. Duine, New perspectives for Rashba spin–orbit coupling, Nat. Mater. **14**, 871 (2015).

[13] V. Mourik, K. Zuo, S. M. Frolov, S. R. Plissard, P. P. A. M. Bakkers, and L. P. Kouwenhoven, Signatures of Majorana fermions in hybrid superconductor-semiconductor nanowire devices, Science **336**, 1003 (2012).

[14] B. Braunecker, G. I. Japaridze, J. Klinovaja, and D. Loss, Spin-selective Peierls transition in interacting one-dimensional conductors with spin-orbit interaction, Phys. Rev. B **82**, 045127 (2010).

[15] C. H. L. Quay, T. L. Hughes, J. A. Sulpizio, L. N. Pfeiffer, K. W. Baldwin, K. W. West, D. Goldhaber-Gordon, and R. de Picciotto, Observation of a one-dimensional spin-orbit gap in a quantum wire, Nat. Phys. **6**, 336 (2010).

[16] A. Takayama, T. Sato, S. Souma, T. Oguchi, and T. Takahashi, One-Dimensional Edge States with Giant Spin Splitting in a Bismuth Thin Film, Phys. Rev. Lett. **114**, 066402 (2015).

[17] T. Okuda, K. Miyamoto, Y. Takeichi *et al.*, Large out-of-plane spin polarization in a spin-splitting one-dimensional metallic surface state on Si(557)-Au, Phys. Rev. B **82**, 161410(R) (2010).

[18] J. Park, S. W. Jung, M.-C. Jung, H. Yamane, N. Kosugi, and H. W. Yeom, Self-assembled Nanowires with Giant Rashba Split Bands, Phys. Rev. Lett. **110**, 036801 (2013).

[19] T. Tanaka and Y. Gohda, First-principles prediction of one-dimensional giant Rashba splittings in Bi-adsorbed In atomic chains, Phys. Rev. B **98**, 241409(R) (2018).

[20] Y. Zhang, T.-T. Tang, C. Girit *et al.*, Direct observation of a widely tunable bandgap in bilayer graphene, Nature (London) **459**, 820 (2009).

[21] A. H. Castro Neto, F. Guinea, N. M. R. Peres, K. S. Novoselov, and A. K. Geim, The electronic properties of graphene, Rev. Mod. Phys. **81**, 109 (2009).

[22] H. Zhang, C. Lazo, S. Blügel, S. Heinze, and Y. Mokrousov, Electrically Tunable Quantum Anomalous Hall Effect in Graphene Decorated by 5d Transition-Metal Adatoms. Phys. Rev. Lett. **108**, 056802 (2012).

[23] E. -J. Kan, Z. Li, J. Yang *et al.*, Will zigzag graphene nanoribbon turn to half metal under electric field? Appl. Phys. Lett. **91**, 243116 (2007).

[24] Y.-W. Son, M. L. Cohen, and S. G. Louie, Half-metallic graphene nanoribbons, Nature (London) **444**, 347 (2006).

[25] Z. Qin, G. Qin, B. Shao, and X. Zuo, Unconventional magnetic anisotropy in onedimensional Rashba system realized by adsorbing Gd atom on zigzag graphene nanoribbons, Nanoscale **9**, 11657 (2017).

[26] P. E. Blöchl, Projector augmented-wave method, Phys. Rev. B **50**, 17953 (1994).

[27] G. Kresse and J. Furthmüller, Efficiency of *ab-initio* total energy calculations for metals and semiconductors using a plane-wave basis set, Comput. Mater. Sci. **6**, 15 (1996).

[28] J. P. Perdew, K. Burke, and M. Ernzerhof, Generalized Gradient Approximation Made Simple, Phys. Rev. Lett. **77**, 3865 (1996).

[29] S. L. Dudarev, G. A. Botton, S. Y. Savrasov, C. J. Humphreys, and A. P. Sutton, Electron-energy-loss spectra and the structural stability of nickel oxide: An LSDA+U study, Phys. Rev. B **57**, 1505 (1998).

[30] V. I. Anisimov and O. Gunnarsson, Density-functional calculation of effective Coulomb interactions in metals, Phys. Rev. B **43**, 7570 (1991).

[31] P. Larson and W. R. L. Lambrecht, Electronic structure of Gd pnictides calculated within the approach, Phys. Rev. B **74**, 085108 (2006).

[32] J. Neugebauer and M. Scheffler, Adsorbate-substrate and adsorbate-adsorbate interactions of Na and K adlayers on Al (111), Phys. Rev. B **46**, 16067 (1992).

[33] G. Makov and M. C. Payne, Periodic boundary conditions in ab initio calculations, Phys. Rev. B **51**, 4014 (1995).

[34] G. H. O. Daalderop, P. J. Kelly, and M. F. H. Schuurmans, First-principles calculation of the magnetocrystalline anisotropy energy of iron, cobalt, and nickel, Phys. Rev. B **41**, 11919 (1990).

[35] See Supplemental Material at http://link.aps.org/supplemental/10.1103/PhysRevB.101.014451 for the geometry structures, spin density, the convergence curve of MAE vs k mesh and the considered directions of spin axis, which includes Ref. [44].

[36] T. Suzuki, Perpendicular magnetic recording–Its basics and potential for the future, IEEE Trans. Magn. **20**, 675 (1984).

[37] J. Hu and R. Wu, Control of the Magnetism and Magnetic Anisotropy of a Single-Molecule Magnet with an Electric Field, Phys. Rev. Lett. **110**, 097202 (2013).

[38] K. Nakamura, R. Shimabukuro, Y. Fujiwara, T. Akiyama, T. Ito, and A. J. Freeman, Giant Modification of the Magnetocrystalline Anisotropy in Transition-Metal Monolayers by an External Electric Field, Phys. Rev. Lett. **102**, 187201 (2009).

[39] T. R. Dasa, P. Ruiz-Díaz, O. O. Brovko, and V. S. Stepanyuk, Tailoring magnetic properties of metallic thin films with quantum well states and external electric fields, Phys. Rev. B **88**, 104409 (2013).

[40] K. Sakamoto, T. Oda, A. Kimura, K. Miyamoto, M. Tsujikawa, A. Imai, N. Ueno, H. Namatame, M. Taniguchi, P. E. J. Eriksson, and R. I. G. Uhrberg, Abrupt Rotation of the Rashba Spin to the Direction Perpendicular to the Surface, Phys. Rev. Lett. **102**, 096805 (2009).

[41] J. Ibañez-Azpiroz, A. Eiguren, and A. Bergara, Relativistic effects and fully spin-polarized Fermi surface at the Tl/Si(111) surface, Phys. Rev. B **84**, 125435 (2011).

[42] M. Cinal and D. M. Edwards, Magnetocrystalline anisotropy in Co/Pd structures, Phys. Rev. B **55**, 3636 (1997).

[43] S. E. Barnes, J. Ieda, and S. Maekawa, Rashba spin-orbit anisotropy and the electric field control of magnetism, Sci. Rep. **4**, 4105 (2014).

[44] N. N. Negulyaev, V. S. Stepanyuk, W. Hergert, and J. Kirschner, Electric Field as a Switching Tool for Magnetic States in Atomic-Scale Nanostructures, Phys. Rev. Lett. **106**, 037202 (2011).